Available online at www.sciencedirect.com
ScienceDirect
Journal of the European Ceramic Society 27 (2007) 4421–4424
www.elsevier.com/locate/jeurceramsoc

Structural and electrochemical features of Bi_2O_3-based fast oxide ion conductors

V. Fruth *, G. Dobrescu, V. Bratan, C. Hornoiu, S. Preda, C. Andronescu, M. Popa

Institute of Physical Chemistry, 202 Splaiul Independentei, Bucharest 060021, Romania

Available online 19 April 2007

Abstract

Oxide ion conductors have been increasingly studied for many years because of their application in devices with high economical impact such as solid oxide fuel cells (SOFC), oxygen sensors, and dense ceramic membranes for oxygen separation, and membrane reactors for oxidative catalysis. New fast oxide ion conductors for low temperature applications (400–600 °C) have been proposed during recent years.

The influence of Sb_2O_3 and Ta_2O_5 as on the Bi_2O_3 structures and the corresponding electrical behavior were investigated. The powder products, obtained by solid state reactions, were characterized by XRD and SEM. They were sintered at different temperatures and the bulk ceramics were characterized and their electrical behavior versus temperature were recorded.

This investigation underlines the influence of the nature of dopants on the structures and electrical performances bismuth based oxides. For microstructure analysis the theory of fractals was used.

Keywords: Powders-solid state reaction; Grain boundaries; Electronic microscopy; Impedance; Bi_2O_3

1. Introduction

In their original work, Takahashi et al.[1] demonstrated that the high temperature phase with high ionic conductivity can be stabilized to lower temperatures in a similar way as known for cubic zirconia, i.e. by substitution of aliovalent cations for Bi. Bismuth oxide easily forms solid solutions with many other metal oxides. Different structures are found, including fcc, rhombohedral and tetragonal structures on the Bi_2O_3-rich side of the binary systems.[2,3] The stability region of the high ionic conductivity phases can be extended to room temperature by incorporation of lanthanides or transitional oxides up to 45 mol%. Although the δ-phase of Bi_2O_3 exhibits the highest oxide ion conductivity known so far, its use is limited because it is stable only in the narrow temperature range 1002–1097 K. On the other hand Levin and Roth found that the thermal expansion coefficients were by two times lower than those from high-temperature X-ray investigations. Transition from δ- to β-phase is accompanied by a large sudden volume change and by a deterioration of the mechanical properties of the material. The fcc phase of Bi_2O_3, is stabilized by cations with smaller radii than Bi^{3+} and relatively high concentrations. The stabilization of the high temperature phase structure occurs by a contraction of this structure due to the substituent. If the difference between the ionic radius of Bi^{3+} (0.111 nm) and the substituted Ln^{3+} is large, the substitution will result in a large distortion of the host lattice and only a small amount of substituent is necessary for supplying the energy required to stabilize the fcc phase of Bi_2O_3. Conversely, a small difference between the ionic radii of Bi^{3+} and Ln^{3+} requires a large amount of substituent to stabilize the fcc phase. A too large difference between the ionic radii of the Ln^{3+} and Bi^{3+} ions makes the fcc phase unstable.

To prevent some of the disadvantages of Bi_2O_3, the influence of the dopants (antimony or tantalum oxide) on the structure–microstructure of Bi_2O_3 and its electrical behavior were investigated. For microstructure analysis the theory of fractals was used.

2. Experimental

Bi_2O_3 (Fluka 99%) and Sb_2O_3 (Merck 99%) and Ta_2O_5 (Merck 99%) were mixed in stoichiometric proportions to form $Bi_{1.9}M_{0.1}O_x$ (M = Sb or Ta) mixture. The samples were repeatedly grounded in a mortar with pestle to remove any present agglomerates, then pressed into discs of 10 mm diameter and

* Corresponding author.
E-mail address: vfruth@icf.ro (V. Fruth).

0955-2219/$ – see front matter © 2007 Elsevier Ltd. All rights reserved.
doi:10.1016/j.jeurceramsoc.2007.02.174

sintered at different temperatures up to 850 °C and cooled in the furnace down to room temperature.

The structure of the obtained materials was determined by X-ray diffraction (XRD). The XRD patterns were recorded with a standard D5000 Siemens Diffractometer θ–2θ equipped with a graphite monochromator using Cu Kα radiation ($\lambda = 1.5405$ Å) operating at 40 mA and 40 kV. Thermal analysis (DTA/TG) was realized with a Mettler Toledo 851^e equipment, in non-isothermal conditions, in air. The powder morphology and the microstructure of sintered samples were determined by scanning electron microscopy with a Scanning microscope Zeiss DSM 942 equipped with a Link Energy Dispersive X-ray system. The structural observation is correlated with bulk ceramic characteristics (density, porosity) and their electrical behaviour versus temperature. Electrical behavior of the doped Bi_2O_3 ceramic was carried on with an impedance analyzer Wayne Kerr 6440A, in the frequency range 20 Hz–3 MHz, for an applied signal of 100 mV. Silver paste is used as electrode and the data were recorded to following temperatures: 293, 373, 473, 573, 673 and 773 K.

3. Results and discussion

The DTA/TG analyses of the starting mixture were carried out in non-isothermal conditions (Fig. 1a and b). A small mass gain up to 250 °C in the presence of tantalum oxide and 350 °C, respectively, for antimony doped sample was observed. This phenomenon can be correlated with gas adsorption on the powders. Some remarks can be made on Sb doped samples: (i) a small exothermal event, associated with the oxidation of Sb^{3+} to Sb^{5+} at 520 °C and (ii) in the temperature range of 520–560 °C, TG curves recorded a weight loss associated with an endothermic event on the DTA. At higher temperatures, the position of the effects for Ta doped samples shifts to higher values. Detailed investigations were presented in a previous paper.[4,5] The microscopic observations at high temperatures were in good agreement with the DTA data.[4]

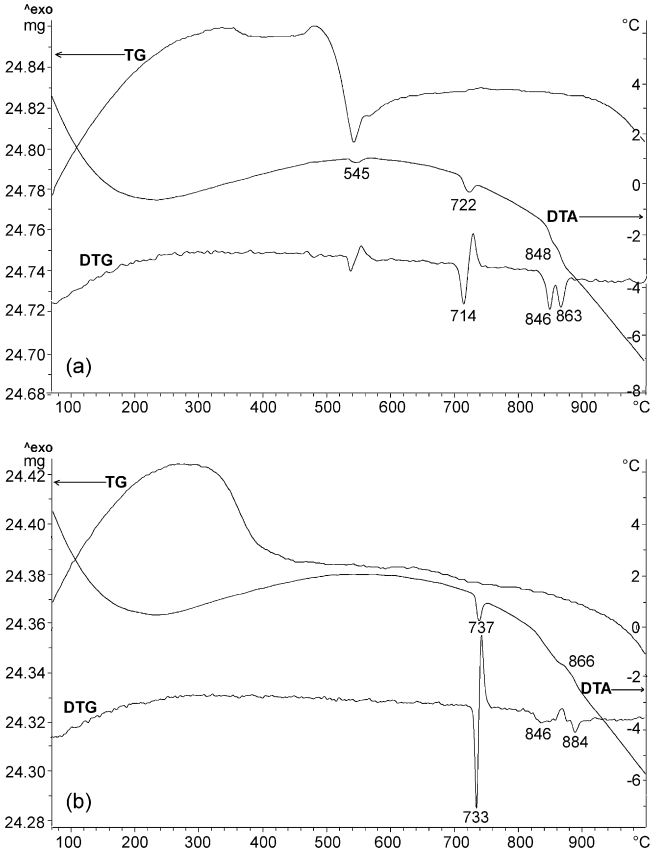

Fig. 1. DTA/TG curves of the starting mixture – $0.95Bi_2O_3 + 0.05Sb_2O_3$ (a) and $Bi_2O_3 + Ta_2O_5$ (b) – up to 1000 °C.

The XRD patterns of $Bi_{1.9}M_{0.1}O_{3-x}$ solid solution, obtained after different annealing treatments, were reported in detail in a previous paper.[5] All samples contained a phases mixture, β*Bi_2O_3 (* mean an impure phase) main phase (β-Bi_2O_3 type phase) and γ*Bi_2O_3 (γ-Bi_2O_3 type phase) designed tetragonal and respectively cubic ($a > 10$ Å) phases. According to Fries et al.[6] when the contents of the guest oxides were very low, a metastable high temperature phase was produced, which can be derived as the $\sqrt{2} \times \sqrt{2} \times 1$ superstructure from δ-Bi_2O_3. The cubic γ*Bi_2O_3 phase [SG: I23 (197)], the second one, is actually a mixture of phases with the cell parameter in the range 10.08–10.26 Å. These values were influenced by the content in dopant and the annealing temperature. That infers that a substitution of the Bi^{3+}—1.03 Å CN6[7] ion by smaller substituted ions (solid solution) takes place. The presence of cubic phase (γ-Bi_2O_3 based type), in small quantities, can be related also with the presence of liquid phase in the system, inferring that this phase crystallised from the melt on cooling.

From SEM images one can observe the influence of substituted oxide on the morphology of samples. Significant changes may be noticed. In antimony doped samples, annealed at 830 °C/20 h, a homogenous microstructure composed of big grains – β*-phase – (∼50 μm) with well-defined polygonal boundaries were obtained (Fig. 2). The porosity is not present in the inter-granular area. The second phase (needle shape) can be assigned to a metastable γ-type bismuth oxide phase. From the EDAX image one can notice that a good dispersion of the atom species is obtained. The boundary and surface liquid phase explain both the bodies contraction at lower temperature and the very good connection between grains after sintering. In the case of Sb doped samples this mechanism is better evidenced. A different process occurred for Ta doped samples. The observed grains present curved edges at 850 °C and a very good connection between them at 870 °C without porosity (Fig. 3).

3.1. SEM images analysis

Self-similarity is the property of an object to look the same when zooming it.[8,9] In the following analysis we shall use the "box counting" method[10–12] to compute the fractal dimension of the contour SEM images and, also we shall compute the fractal dimensions of the grey-level SEM images, converting the grey level of each pixel in height, and computing fractal dimension of the corresponding fractal surface.

For this second goal we shall use the variable length scale method, proposed by Chauvy et al.[13]

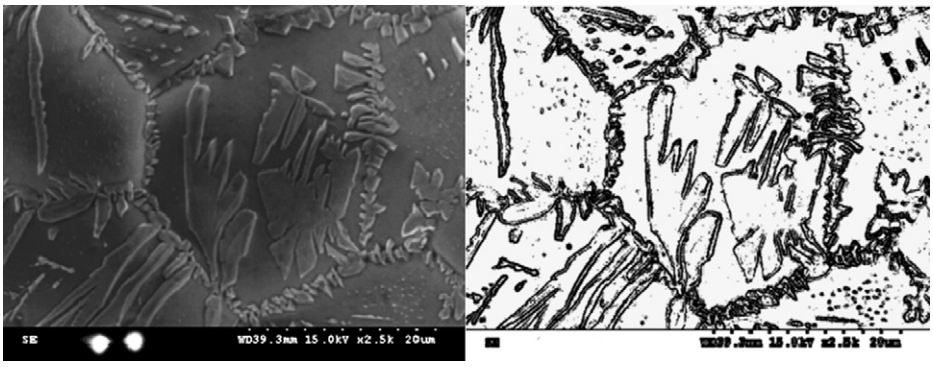

Fig. 2. SEM image (left) and the contour SEM image (right)—sample ($Bi_{1.9}Sb_{0.1}O_x$).

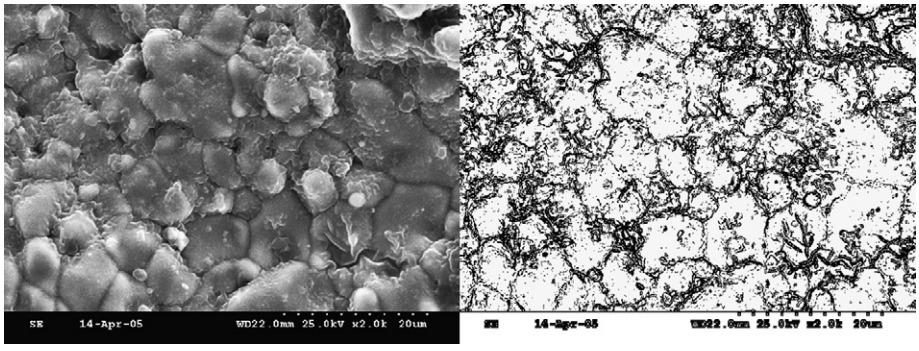

Fig. 3. SEM image (left) and the contour SEM image (right)—sample ($Bi_{1.9}Ta_{0.1}O_x$).

The black and white contour images together with the grey-level SEM images are presented in Figs. 2 and 3. The contour images were obtained finding edges of the surface structures and converting them to black pixels, meanwhile the other pixels that are not from the edge are converted to white pixels.

The contour images of the Sb-doped Bi_2O_3 samples exhibit fractal behavior over a large enough scale range (80–2000 nm) and they are characterized by fractal dimensions 1.60 ± 0.01, linear correlation coefficient of 0.998. The obtained value is closed to the typical fractal dimension (1.71) of a diffusion-limited aggregation cluster embedded in a bi-dimensional Euclidean space.[14] A second method—the variable length scale method was used to compute fractal dimension of the grey-level SEM image. The grey-level of each pixel was assigned to a height value, obtaining a topographic image of the sample. All surfaces exhibit fractal behavior at the micrometric scale (1.6–17.6 μm) with fractal dimensions around 2.82 ± 0.04, indicating self-affine surface with higher correlated points.

The Ta-doped Bi_2O_3 samples also exhibit fractal behavior: the contour images are characterized by a fractal dimension of 1.50 ± 0.05 (100–900 nm), linear correlation coefficient 0.996 and the topographic images by a fractal dimension of 2.59 ± 0.06 (400–8000 nm). Both values are lower than the values obtained for Bi–Sb samples, indicating smoother surfaces and domain edges.

Electrical behavior of the doped Bi_2O_3 ceramic were carried on with an impedance analyzer in the frequency range 20 Hz–3 MHz.

The impedance curves of the two characterized materials ($Bi_{1.9}Sb_{0.1}O_x$ and $Bi_{1.9}Ta_{0.1}O_x$, respectively) have the same profile, mainly a semicircles (Fig. 4). One may say that the intergranular boundaries did not influence the conductivities in the

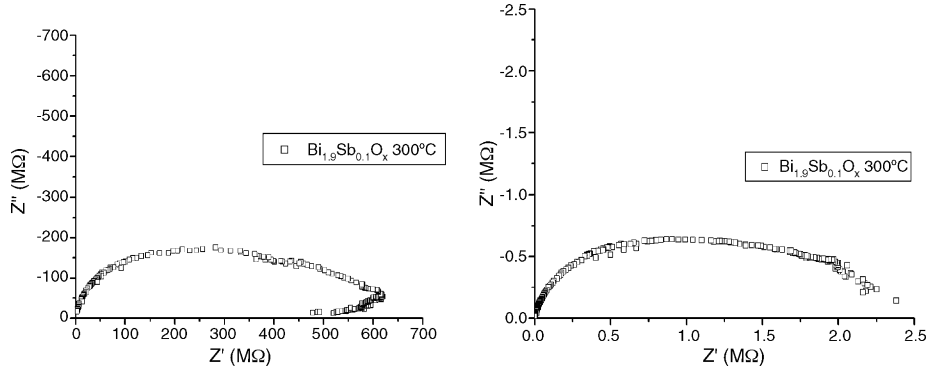

Fig. 4. Impedance data plot for $Bi_{1.9}Sb_{0.1}O_x$ ceramics (left) and $Bi_{1.9}Ta_{0.1}O_x$ (right) at 300 °C.

investigated range of frequencies. In both cases the impedance decreased with the increasing of temperatures. These values are comparable.

At 573 K one may notice a deformation of the semicircle and a bigger angle of tilt. Starting from this temperature the influence of the electrodes has to be mentioned, much more visible at 673 and 773 K, respectively. In the last case the semicircles shift to higher frequencies and cannot be seen in this range of our measurement.

With a ZView 2 software we recorded the bulk resistances for temperatures up to 673 K. Representing the graphic $\ln(1/R) = f(1/T)$ one can observe the existence of two linear domains. The calculated activation energies in the temperature range of 473–673 K for the two ceramic materials have comparable values: $E_a = 0.998$ eV/mol for Ta doped Bi_2O_3 and 1.069 eV/mol for Sb doped Bi_2O_3, respectively.

4. Conclusion

The influence of two dopants (Sb_2O_3 or Ta_2O_5—5% mole ratio) on microstructure and properties of thermal treated Bi_2O_3 were investigated.

The nature of dopants influenced the behaviour of the starting mixture in non-isothermal condition, Sb_2O_3 and Ta_2O_5 enlarging the stability domain of δ-Bi_2O_3 phase. The melting point of Ta doped Bi_2O_3 is over 900 °C.

The phases presented in the annealed samples consist of a major one, with tetragonal symmetry, and a second one with cubic symmetry, localised especially in the boundary area and related with the liquid phase presence.

SEM/EDAX shows a good sintered bodies. The presence of antimony oxide promotes a uniform dimensionality of the grains (∼50 μm). All surfaces exhibit fractal behavior at the micrometric scale with fractal dimensions, indicating self-affine surface with higher correlated points. The Ta-doped samples present lower fractal values than Sb-doped samples, indicating smoother surfaces and domain edges.

The electric conductivity is influenced also by the nature of dopants. The results are in good agreement with structural and morphological observation.

References

1. Takahashi, T., Iwahara, H. and Nagai, Y., High oxide ion conduction in sintered Bi_2O_3 containing SrO, CaO or La_2O_3. *J. Appl. Electrotherm.*, 1972, **2**, 97–104.
2. Levin, E. M. and Roth, R. S., Polymorphism of bismuth sesquioxide. II. Effect of oxide additions on the polymorphism of Bi_2O_3. *J. Res. Nat. Bur. Stand.*, 1964, **68A**, 197–206.
3. Hund, F., Fluoritmischphasen der Dioxide von Uran, Thorium, Cer und Zirkonium mit Wismutoxid. *Z. Anorg. Allg. Chem.*, 1964, **333**, 248–255.
4. Fruth, V., Popa, M., Berger, D., Ionica, C. M. and Jitianu, M., Phases investigation in the antimony doped Bi_2O_3 system. *J. Eur. Ceram. Soc.*, 2004, **24**, 1295–1299.
5. Fruth, V., Ianculescu, A., Berger, D., Preda, S., Voicu, G., Tenea, E. *et al.*, Synthesis, structure and properties of doped Bi_2O_3. *J. Eur. Ceram. Soc.*, 2006, **26**, 3011–3016.
6. Fries, T., Lang, G. and Kammerling-Sack, S., Defect fluorite structures in the Bi-rich part of the system Bi_2O_3–Re_2O_3. *Solid State Ionics*, 1996, **89**, 233–240.
7. Shannon, R. D., Revised effective ionic radii and systematic studies of interatomic distances in halides and chalcogenides. *Acta Cryst. A*, 1976, **32**, 751–767.
8. Mandelbrot, B. B., *Fractals: Form, Chance and Dimension*. Freeman, San Francisco, 1977.
9. Mandelbrot, B. B., *The Fractal Geometry of Nature*. Freeman, San Francisco, 1982.
10. Pfeifer, P. and Obert, M., *The Fractal Approach to Heterogeneous Chemistry: Surfaces Colloids and Polymers*. J. Wiley & Sons Ltd., New York, 1989, pp. 11–43.
11. Grassberger, P., On the fractal dimension of the Henon attractor. *Phys. Lett. A*, 1983, **97**, 224–226.
12. Samios, J., Pfeifer, P., Mittag, U., Obert, M. and Dorfmuler, Th., Brownian motion and fractal geometry in the liquid state: translation of linear molecules. *Chem. Phys. Lett.*, 1986, **128**, 545–550.
13. Chauvy, P. F., Madore, C. and Landolt, D., Variable length scale analysis of surface topography: characterization of titanium surfaces for biomedical applications. *Surf. Coat. Technol.*, 1998, **110**, 48–56.
14. Barabasi, A.-L. and Stanley, H. E., *Fractal Concepts in Surface Growth*. Cambridge University Press, Cambridge, UK, 1995, p. 179.